Chemical Geology 661 (2024) 122156

Contents lists available at ScienceDirect

Chemical Geology

journal homepage: www.elsevier.com/locate/chemgeo

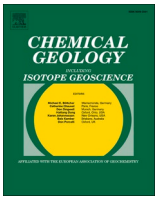

A case study of depolymerization in silicates: Melting of quartz and zircon crystallization at high pressure

A. Sánchez-Navas [a,*], S. Melchor [b], J. Ortega-Castro [c], I. Vidal-Daza [b], A. Castro [d]

[a] Departamento de Mineralogía y Petrología, Universidad de Granada, Granada 18071, Spain
[b] Grupo de Modelización y Diseño Molecular, Facultad de Ciencias, Universidad de Granada, Granada 18071, Spain
[c] Departamento de Química-Física, Universidad de las Islas Baleares, Palma de Mallorca 07071, Spain
[d] Museo Nacional de Ciencias Naturales, C.S.I.C., Madrid 28006, Spain

ARTICLE INFO

Editor: Claudia Romano

Keywords:
Depolymerization
Melting of quartz
Zircon crystallization
SiO bond
Bowen's reaction series

ABSTRACT

The experimental study of depolymerization reaction $SiO_2 + ZrO_2 \rightarrow ZrSiO_4$ reveals that melting of quartz and crystallization of zircon in the presence of water increases at high pressure. The melting rate of quartz is identified as the rate-determining step of the reaction. In highly polymerized silicates, Si-O-Si bond angles are subject to alteration under the influence of pressure. This phenomenon is particularly noticeable within the three-dimensional lattice structure of quartz, where each corner of the tetrahedra is shared. Theoretical analysis of the Si-O-Si bond angle bending demonstrates a change in oxygen hybridization from *sp* to sp^2, favoring larger Si-O distances. The sp^2 hybridization in bridging oxygen promotes acid attack by hydrogen ions of water, resulting in SiO bond heterolysis in quartz. The depolymerization from tectosilicates to nesosilicates leads to an increase in oxygen "size" and polarizability, as well of closer packing of oxygen atoms. This change in behavior and packing of oxygens is further illustrated by the high-pressure-driven transition from tridymite to stishovite. Additionally, the impact of network-modifying elements on the structure of polymerized silicates is investigated; particularly those acting as electron donors, which lengthen Si-O distances in quartz. The findings are discussed in relation to key topics in Earth Sciences, including the crystal chemical basis of the Bowen's reaction series, the "metallization" in rocky planets and the structural controls of hydrous and dry melting in silicates.

1. Introduction

The degree of polymerization of silicate minerals and melts (tetrahedral connectivity) controls their compressibility and increases during decompression after magma ascent to shallow crustal levels. Silicon forms silica tetrahedra (one silicon bonded to four oxygens on the vertices of a tetrahedron) in silicate crystals and melts under low pressure. Nevertheless, silica octahedra occur at higher pressure. Silica tetrahedra may link together forming tetrahedral groups that may share two, three or four oxygen atoms, giving rise to a Si-O-Si network or "structural skeleton" (polymerization), which is responsible of the acid character of silicate crystals and melts. Elements that combine with oxygen to form basic oxides have higher coordination number than silicon in silicate structures. They are considered network-modifying elements. In particular, the oxides of monovalent cations (namely, K_2O and Na_2O) and water affect drastically the Si-O-Si network and favor the formation of silicate crystals and melts with a less polymerized structure (Kushiro, 1975). Thermodynamic analyses of depolymerization reactions caused by network-modifiers show that destabilization of the Si-O-Si network structure may be checked by the activity coefficient of SiO_2 (γ_{SiO2}; Hirschmann et al., 1998). The structure of pure SiO_2 liquid or solid, in which tetrahedra are all bonded to four other silicate tetrahedra, is representative of the standard state. Thus, the silica activity (a_{SiO2}) in multicomponent silicate systems is a measure of the polymerization degree in this approach. Hirschmann et al. (1998) have explored quantitatively the relationships between γ_{SiO2}, melt composition and pressure in lherzolite-saturated liquids in the NCMAS system, showing a smooth decrease in γ_{SiO2} with increasing X_{Na2O} at constant temperature and pressure, and a more pronounced decrease in γ_{SiO2} for Na-free liquids with increasing pressure from 0.7 to 3.4 GPa. Moreover, γ_{SiO2} is so low at high pressure that the effect of alkalis on γ_{SiO2} is not observed for pressures above 3 GPa (see Fig. 6A of Hirschmann et al., 1998).

The differentiation of chemical species, SiO_2 in particular, within

* Corresponding author.
E-mail address: asnavas@ugr.es (A. Sánchez-Navas).

https://doi.org/10.1016/j.chemgeo.2024.122156
Received 31 January 2024; Received in revised form 26 April 2024; Accepted 11 May 2024
Available online 17 May 2024

planetary interiors is primarily controlled by melting and crystallization processes, which are intimately linked to evolution histories of the planets (Kushiro and Mysen, 1992). Understanding the structural response of silicate crystals and melts to pressure and composition is crucial in earth and planetary sciences. Bending of Si-O-Si bond angles is an essential geometrical mechanism in the structural compression of highly polymerized silicates with depth (*e.g.* Hazen et al., 1989 and references therein). Tightening of the inter-tetrahedral bond angle with increasing pressure is followed by breakdown of the tetrahedral connectivity with an increase of density (Wang et al., 2014).

Depolymerization of the Si-O-Si network structure by metal oxides (M), that is usually expressed by the acid-base reaction Si-O-Si + M-O-M → 2Si-O-M, may be also written as a reaction involving oxygen atoms of different softness or polarizability: $O^0 + O^{2-} \rightarrow 2O^-$ (Hess, 1977). The significance of the bond at the oxygen atom and its coordination has been demonstrated by Burdett and McLarnan (1984) and Burdett (1995) in their orbital interpretation of Pauling's second and third rules. Burdett and McLarnan (1984) have established a correlation between the band structure energies of crystals and the energies computed for an anion coordination polyhedron. These authors have emphasized the importance of the environment of anions where most of the valence electrons are found. The nature of bond at oxygen atom has been traditionally expressed through the concept of oxygen hybridization (Fyfe, 1954). According to this author, the oxygen hybridization in SiO bonds decreases as the bond strength shifts from the *sp* to sp^3 end member hybrids, where all possible combinations of *s* and *p* electrons hybrids exist. It appears that superior oxygen hybridization in SiO bonds is associated with a lower average coordination number of the oxygen anion bonded to Si (Brown and Gibbs, 1969). This is especially true when oxygen adopts a *sp* linear hybrid with a significant proportion of *s* character in these bonds.

The process of zircon crystallizing from melted quartz is an example of depolymerization. This study experimentally investigates the progression of the reaction Si-O-Si + Zr-O-Zr → 2Si-O-Zr under pressure in the presence of water. Zirconium was selected over other electron donor atoms (cations) due to its high ionic potential. The major driving force for Si-O-Si + M-O-M → 2Si-O-M is expected to be the covalent stabilization of the ZrO bond, rather by any type of OM ionic interaction.

Quantum mechanical calculations have been performed to investigate the mechanism of depolymerization. The Quantum Theory of Atoms in Molecules (QTAIM) (Bader, 1990) and the Electron Localization Function (ELF) (Silvi and Wagner, 1997) are employed to explore the relationship between the Si-O-Si angle and the Si-O distance. Initially, the destabilization of the SiO bond due to bending of the Si-O-Si bond angle under pressure (geometrical perturbation) is analyzed. Additionally, the lengthening of Si-O bond distances due to network-modifying elements (electronegativity perturbation) is studied. Finally, the transition from open framework structures to close packed structures in silicates is investigated and related to a change in the nature (basicity) of the oxygen atoms in a search of a wide concept of depolymerization.

2. Rationale: hard-soft, acid-base approach to depolymerization reactions in silicates

As indicated earlier, the selection of zirconium, a relatively scarce element in Earth's silicate materials, was made due to its distinct electronegative nature as a cation (a high field strength element). This property allows it to form robust bonds with the silicate anion. The influence of the cation's electronegativity on the average strength of the M-O-Si bonds can be assessed through the enthalpy of formation of oxysalts. One example is provided by the isostructural series formed by the carbonates: calcite → magnesite → rhodochrosite → siderite. The enthalpies of formation from elements at reference *T* (25 °C) and *P* (1 bar) have been calculated with Perple_X application (Connolly, 2023). They are −1101.589, −1008.106, −788.076, −659.847 (kJ/mol), respectively and the electronegativity of the involved cations Ca^{2+}, Mg^{2+}, Mn^{2+} and Fe^{2+} are 1, 1.2, 1.55 and 1.83, respectively. Thus, a correlation between enthalpy and electronegativity may be deduced for carbonates.

Ryerson (1985) proposed that depolymerization, resulting from the enrichment of network-modifying cations in silicate melts, leads to a reduction in a_{SiO2}. This phenomenon is primarily controlled by enthalpic effects related to variations in bond energies, rather than entropic effects. According to Ryerson (1985), in depolymerization reactions, bond energies correlate with the polarization of the nonbridging oxygen (NBO) toward the metallic cation. Bonds become stronger as the field strength of the cation increases. Notably, Mg^{2+} and Fe^{2+} exhibit similar sizes and possess the same charge. However, they differ slightly in their second ionization potential: 15 eV for Mg^{2+} and 16.2 eV for Fe^{2+}. As a consequence, the FeO bond exhibits a more covalent character than the MgO bond, with Fe^{2+} acting as a softer acid compared to Mg^{2+}. Consequently, Fe^{2+} favors softer basic silicate environments constituted by isolated tetrahedra. In contrast, the harder acid Mg^{2+} cation prefers more polymerized silicate structures, characterized by chains and sheets of SiO_4 tetrahedra (as discussed by Tossel and Vaughan in 1992, page 428).

This concept aligns with Pearson's theory of hard (strong) and soft (weak) acids and bases (Pearson, 1966; Burdett and McLarnan, 1984). Applying this framework to the exothermic exchange reaction between olivine and pyroxene: $Mg_2SiO_4 + 2FeSiO_3 \rightarrow Fe_2SiO_4 + 2\ MgSiO_3$, we observe that the major driving force lies in the strong covalent stabilization between Fe^{2+} and SiO_4^{4-} (the soft-soft pair). Consequently, Fe-rich silicate minerals with a low degree of SiO_4^{4-} polymerization are expected to crystallize from alkaline melts with a lower degree of polymerization. For instance, fayalite-rich olivine precipitate in dacite, rhyolite and obsidian, and almandine-rich garnets form in dacites (Kushiro, 1975).

On the other hand, silicate minerals with a high degree of polymerization tend to favor Mg. For example, talc predominantly consists of Mg, whereas iron-talc exhibits signs of unstable structure (Ramberg, 1952).

According to Lewis's concepts, a base is characterized as an atom or molecule with the capacity to donate electrons to the Si-O-Si network structure found in silicate crystals and melts. Mulliken and Pearson (1969) further translated the acid and base framework into the language of quantum mechanics: a base is a species that utilizes a doubly occupied orbital to initiate a reaction, whereas an acid relies on an empty orbital for the same purpose. The donor orbital in the base is usually the highest occupied molecular orbital (HOMO), and the acceptor orbital in the acid is usually the lowest unoccupied molecular orbital (LUMO; HOMO and LUMO being known as frontier orbitals). Soft acids are characterized by low-lying acceptor orbitals (electronegative cations) and soft bases by high-lying donor orbitals (electropositive anions; Burdett and McLarnan, 1984). Simple perturbation molecular orbital theory predicts that for two interacting orbitals of suitable symmetry and overlap (as occurs in an acid-base reaction, for example), the smaller the difference in the orbital energies, the greater the covalent interaction (Jensen, 1980, page 113) is.

The interaction between cations and anions can arise from perturbations involving the $LUMO_{acid}$ (Lowest Unoccupied Molecular Orbital of the acid) and the $HOMO_{base}$ (Highest Occupied Molecular Orbital of the base). Specifically, when dealing with electronegative cations (referred to as “soft acids”) and electropositive anions (“soft bases”), we anticipate a more covalent stabilization.

The basicity of a molecule (or solid) correlates with the energy of the frontier orbitals. This concept, as discussed by DeKock and Barbachyn (1979)and Dekock and Gray (1989), sheds light on the behavior of silicate crystals and melts. Notably, the SiO antibonding orbitals represent the highest-energy or frontier orbitals within these materials.

When these orbitals are populated with valence electrons -often contributed by alkali or alkaline-earth metals and others electron-donor

network-modifiers (such as H_2O), the basic character of silicate crystals and melts undergoes a dramatic increase. Consequently, resulting structures can be stabilized through distortions, wherein SiO bonds are broken, leading to a process known as depolymerization (as discussed by Burdett in 1980, page 265, and Tossel and Vaughan in 1992, page 358).

So, the process of depolymerization of silicates structures from tectosilicates to nesosilicates may be related to the destabilization of the SiO bond due to population of the SiO antibonding orbitals. The electron population of the SiO antibonding orbitals (and basicity of the silicate crystals and melts) could be measured by the number of valence electron per atom (electron count; Burdett, 1980, page 265). The acid-base character of a silicate structure is determined by the ratio of the number of electrons in the anions to the number of Oxygen (O) and Silicon (Si) atoms in the silicate anion group, which are the electronegative atoms in the structure. Consequently, the number of electrons per atom varies. For instance, in three-dimensional structures such as quartz, which is acidic, the ratio is 5.33. On the other hand, in isolated tetrahedra like orthosilicates (*e.g.,* olivine), which are basic, the ratio is 6.4.

Fig. 1A illustrates the relationship between the energy of Mg- and Fe-silicate formation, as measured by enthalpy, and the strength of their respective acids, as indicated by the electron count. It is observed that the strongest acids yield higher enthalpies of formation with MgO or FeO. The softness (or polarizability) of the anion, as determined by the electron count, decreases in the following order: SiO_4^{4-} (isolated) → SiO_3^{2-} (single chain) → $Si_2O_5^{2-}$ (sheet). Fig. 1A also demonstrated how the softness of a metallic oxide, which increases with the electronegativity of the cation (from Mg to Fe), results in less negative enthalpies of formation. Amphiboles are excluded from this figure due to issues related to their thermodynamic data. However, the impact of the difference in electronegativity between Fe and Mg on the enthalpies of formation from the elements for this mineral family is also evident (*e.g.* the formation enthalpies of anthophyllite and Fe-anthophyllite, calculated with Perple_X (Connolly, 2023), are −11,183.15 and − 8752.42 kJ/mol, respectively). The influence of electronegativity of Ca, Mg, Zr, Mn and Fe cations, according to Pauling's scale (Jensen, 1996), on the calculated enthalpies of formation along the nesosilicate series larnite → monticellite → forsterite → zircon → tephroite → fayalite is clearly depicted in Fig. 1B.

3. Melting of quartz and precipitation of zircon at high pressure

The reaction of quartz and baddeleyite to form zircon at (constant) high-temperature and under different pressure conditions has been investigated in a piston-cylinder apparatus (see Appendix A). In relation to the nature of the starting material and the specific preparation of the capsules for that reaction, two experimental designs were used: 1) In Experiments A, quartz pellets were surrounded by a powder of baddeleyite. In turn, both the quartz core and its baddeleyite rim were included in a basanite powder matrix (composition of basanite volcanic rock in Table 1). 2) In Experiments B, quartz pellets were found directly within a matrix formed by the basanite powder supplemented with a 2% of ZrO_2. Water was added in both cases (10 wt%). In both types of experiments, the temperature was fixed at 1000 °C and the pressures assayed were 0.3 GPa (Experiments A-1, B-1) and 2 GPa (Experiments A-2, B-2). All experiments lasted 48 h. The use of quartz as pellets of around 1 mm in diameter guaranteed a low rate for the supply of silica to the reaction, and therefore favored the formation of larger zircon crystals. In addition, the large size of pellets allowed a clear observation of the reaction front during the melting process that affected the quartz particle. Basanite matrix was employed because of its low silica content and relatively high content of alkalis (Table 1). Alkalis favored the melting of the three-dimensional network of quartz. The low SiO_2 content of basanite induced dissolution of ZrO_2 in the melt. High ZrO_2 concentrations are achieved in mafic magmas, as evidenced by the experimental works of Bea et al. (2022), which demonstrated that zircon solubility in silicate melts increases exponentially with decreasing silica. Water was added in the experiments to produce depolymerized melts rich in dissolved water. Water-saturated melts are more fluid and conductive to diffusion than a dry melt, thus favoring the growth of larger zircon crystals.

In Experiment A-1, the back-scattered electron images obtained from polished sections of the experimental capsules in the baddeleyite rim show that zircon did not growth at 0.3 GPa (Fig. 2A), while many zircon crystals formed at 2 GPa in Experiment A-2 (Fig. 2B). Melting of quartz pellets occurred at 2 GPa in Experiments A-2 and B-2. Zircon crystals grew directly from the melt formed within the SiO_2-rich regions occupied by the precursory quartz pellet at 2 GPa in Experiment A-2 (Fig. 2C), where the ZrO_2 necessary for the precipitation of zircon clearly was provided by the surrounding baddeleyite rim. Zircon crystals with skeletal morphologies formed in the basanite matrix supplemented with ZrO_2 at 2 GPa (Experiment B-2, Fig. 2D). However, they did not grow from the melt formed within the SiO_2-rich regions occupied by the precursor quartz pellets at 2GPa in Experiment B-2 (Fig. 2E) or from the scarce silica-rich melts (Table 1) formed at 0.3 GPa in Experiment B-1 (Fig. 2F).

Melting of precursor quartz pellets only occurred at high pressure (Experiments A-2 and B-2). This process was enhanced by the diffusion/advection of elements from the basanite matrix. After the reaction, these

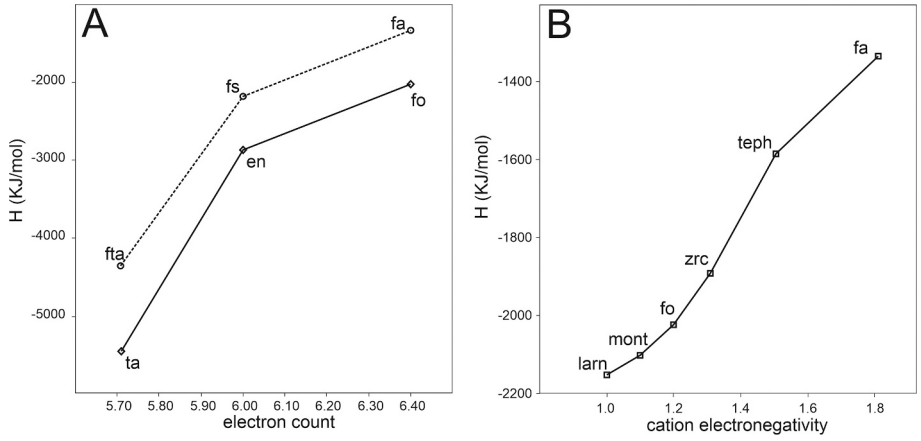

Fig. 1. A) Plot of formation enthalpy (calculated with Perple_X (Connolly, 2023)) *versus* electron count (number of electrons in the anions divided by the number of O and Si atoms of the silicate anion group) for Mg- and Fe silicates (ta: talc, en: enstatite, fo: forsterite, fta: ferro-talc, fs: ferrosilite, fa: fayalite). B) Plot of formation enthalpy *versus* electronegativity of cations (Ca, Mg, Zr, Mn and Fe) in nesosilicate minerals (larnite: larn, monticellite: mont, forsterite: fo, zircon: zrc, tephroite: teph, fayalite: fa).

Table 1
Major-element composition of basanite volcanic rock starting material (column 1) and melts formed from reaction between basanite and quartz pellets at $P = 2$ GPa (Experiment A-2: columns 2 and 3; Experiment B-2: columns 4 and 5) and at $P = 0.3$ GPa (columns 6 and 7). Two single spot analysis were performed by EPMA for melt formed in the experiment. See Appendix A of experimental methods for analytical procedures.

	Basanite	*Melt*					
		P = 2 GPa (A-2)		*P = 2 GPa (B-2)*		*P = 0.3 GPa (B-1)*	
SiO_2	40.132	58.843	59.251	50.464	50.355	72.461	73.239
TiO_2	4.870	0.278	0.275	1.896	1.872	1.499	1.726
Al_2O_3	13.596	15.429	15.168	15.673	15.345	6.053	5.853
Fe_2O_3	17.074	1.551	1.641	5.787	5.497	6.569	6.811
MnO	0.193	0.024	0.052	0.155	0.189	0.112	0.009
MgO	7.598	0.185	0.160	2.670	2.613	0.800	0.841
CaO	10.532	1.398	1.380	5.426	5.607	0.543	0.557
Na_2O	3.282	4.263	3.891	3.485	3.332	2.946	2.897
K_2O	1.490	3.363	3.235	1.971	2.058	3.874	4.012
P_2O_5	0.780	0.011	0.041	0.517	0.537	0.017	0.091
ZrO_2	0.036	0.071	0.034	0.407	0.466	0.562	0.497
	98.575	84.848	84.567	87.373	86.680	93.404	94.540

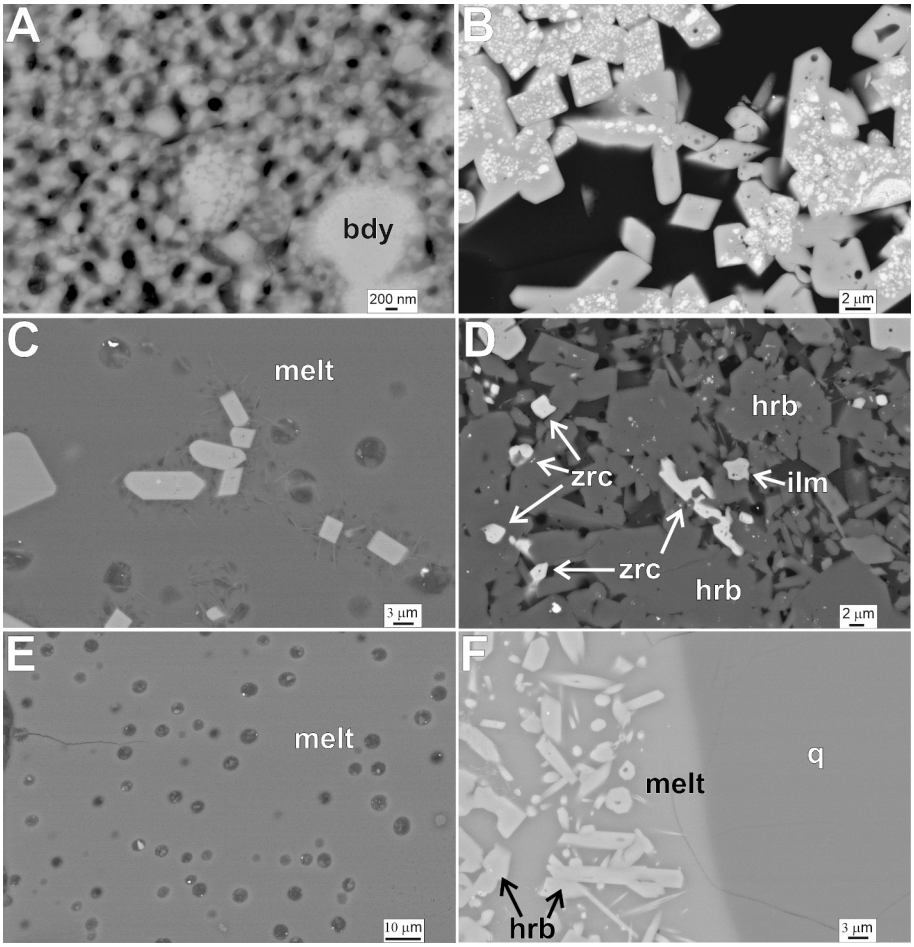

Fig. 2. A) Back-scattered electron image of baddeleyite (bdy) surrounded by an extremely low amount of glass in Experiment A-1 (at $P = 0.3$ GPa). B) Crystals of zircon including minor amounts of baddeleyite in Experiment A-2 (at $P = 2$GPa). C) Zircon crystals precipitated from a melt formed in the region occupied by the precursory quartz pellet in Experiment A-2. D) Skeletal crystals of zircon (zrc) formed together with hornblende (hrb) and ilmenite (ilm) in the basanite matrix at $P = 2$ GPa (Experiment B-2). E) Back-scattered image of a melt formed after complete dissolution of quartz pellets at $P = 2$ GPa (Experiment B-2). F) Detail of the contact between the quartz pellet (q, right) and the basanite matrix, where hornblende crystals (hrb) formed in relation to a scarce silica-rich melt at $P = 0.3$GPa (Experiment B-1).

elements appear to be incorporated into the melt located at the site of the precursor quartz pellets (Table 1). However, the relative contents of elements are different in the melts formed in Experiments A-2 and B-2. Newly formed minerals, that constitute a sink for chemical species, crystallized directly from melt in Experiment A-2 (Fig. 2C). In addition to zircon, newly formed minerals are titanite, ilmenite and hornblende. The relatively high ZrO_2 content (around 0.5 wt%) measured in the melting of Experiments B-1 and B-2 (Table 1) is explained by the absence of newly formed zircons in the liquids resulting from the melting of quartz pellets. No minerals crystallized from melting in Experiment B-2

(Fig. 2E), which is poorer in SiO_2 and H_2O and richer in TiO_2, Fe_2O_3, MgO, P_2O_5 and CaO than melted in Experiment A-2 (Table 1).

Our experimental results show an enhancement of the reaction process with the increase of pressure in the experiments assayed. Quartz pellets appear completely melted in experiments performed at 2 GPa where zircons grew widely from the melt or within the basanite matrix supplemented with ZrO_2. On the other hand, quartz pellets did not melt in the experiments performed at a low pressure. The occurrence of larger amounts of unreacted baddeleyite clots in Experiment A-1 performed at 0.3 GPa (Fig. 2A) than in the Experiment A-2 at 2 GPa (Fig. 2B) shows an exceptionally low supply of silica for the zircon forming-reaction at lower-pressure. Therefore, from a kinetics point of view, dissolution of quartz pellet was the "rate-determining step" in our experimental study of the reaction $SiO_2 + ZrO_2 \rightarrow ZrSiO_4$.

4. The role of water in the melting of quartz at high pressure

The influence of factors such as temperature, water content or the composition of the system on the reaction 1 quartz +1 baddeleyite → 1 zircon was not investigated beyond the aspect of pressure. The Gibbs energy of the reaction, calculated with Perple_X (Connolly, 2023), functions as a pressure-dependent variable at constant temperature (1000 °C). As the Gibbs energy becomes increasingly negative, the reaction progresses more substantially to the right with increasing pressure (Fig. 3A). The pressure dependence of Gibbs energy in the studied reaction primarily arises from the volume change of the reaction and the change in the molar volume of quartz with pressure. Fig. 3B illustrates the significant volume decrease of quartz with increasing pressure at constant temperature, compared to that of baddeleyite. This observation aligns with the fact that silica solubility increases with depth for typical geothermal gradients (Walther and Helgeson, 1977; Spear, 1995, page 661).

While the dissolution of quartz is primarily driven by pressure, the role of water appears to be significant in the depolymerization reaction studied here. The total weight percent from EPMA analysis (Table 1) of the glass found within the regions occupied by the precursor quartz pellets in Experiments B-1 and B-2 indicates a substantial content of water in the melt. The water content can be monitored by the intensity of the band centered near 3500 cm^{-1} in the Raman spectra of these glasses (Fig. 4). Raman shifts at low frequencies, between 100 and 1500 cm^{-1}, are attributed to covalent bonds linking SiO_4 tetrahedra (Neuville et al., 2008; Lenoir et al., 2008). The broad band centered near 3500 cm^{-1} (arrow) corresponds to the water dissolved in the glasses and could be assigned to OH, water, Si-OH and SiO-HOH, and the peak at 1620 cm^{-1} would be bending of water (Le Losq et al., 2012 and references therein). The intensity of this band relative to the intensity of the low-frequency Raman bands is higher in Experiment B-2 (B) than in Experiment B-1 (A). This indicates that the concentration water is higher in silicate glasses formed under high pressure.

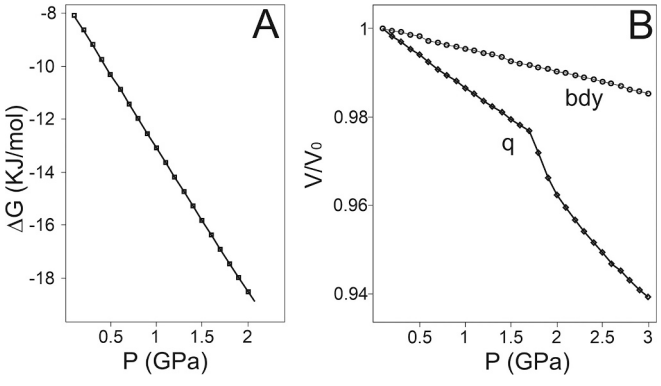

Fig. 3. Change in Gibbs free energy of the reaction 1 quartz +1 baddeleyite → 1 zircon (A) and in molar volume of quartz and baddeleyite (B) with pressure at constant temperature (1000 °C) calculated with Perple_X (Connolly, 2023).

The formation of hydrogen-bridged bonds with oxygen atoms of silicates is facilitated at high-pressure, as evidenced by numerous experimental results of the literature (*e.g.* Johannes and Holtz, 1996). While various models have been proposed for the incorporation of water into silicate melts (Burnham, 1975), the process essentially involves an acid attack by the hydrogen of the water molecules on the oxygen atoms of the silicate anions (Gutmann, 1978). It is well established that the OH bond weakens as oxyacids become progressively stronger (Ramberg, 1952). As demonstrated in Section 2, the bond between oxygen and metal is weak in the salts of strong or hard acids. The weaker the metal-oxygen bond, the stronger the bond between oxygen and nonmetal or metalloid elements, and the higher the enthalpy of salt formation. The Section 2 also shows that as we transition from orthosilicates to metasilicates, the strength of the corresponding oxyacid increases. The fact that the OH bond is weaker in stronger oxyacids leads us to stablished that the more polymerized the silicate structure, the stronger the oxyacids, and the more resistant the silicates are to weathering. This explains the dissolution of common rock-forming silicate minerals under Earth-surface conditions as a function of the degree of connectedness or corner-sharing of [SiO_4] tetrahedra (Velbel, 1999).

In summary, the significant water content in glasses formed in regions occupied by precursor quartz pellets is attributed to an increase in the softening or basic character of the Si-O-Si network with pressure. This explains the presence of glasses with low silica content at 2 GPa (Experiments A-2 and B-2; Table 1), which corresponds to depolymerized melts.

Koch-Muller et al. (2001) have experimentally measured a higher proton affinity for the bridging oxygen atoms as the Si-O-Si angle narrows and the Si—O bond length increases. The decrease in volume with pressure of an "ideal" quartz structure, composed of perfectly regular tetrahedra of fixed volume (Thompson et al., 2011), is approximately equal to the decrease in volume observed for quartz with increasing pressure in many other data sets (*e.g.* Dera et al., 2011). This indicates that in quartz, volume decreases with pressure solely due to the bending of the inter-tetrahedral angle. Therefore, the bending of Si-O-Si bond angle would enhance the ability of water to sever the Si-O-Si links with pressure.

5. Effect of pressure on the Si-O-Si network structure: stability of the SiO bond with Si-O-Si angle bending

As previously noted, the structural compaction of highly polymerized silicates with depth occurs through bending of the Si-O-Si bond angle. A pronounced negative correlation between Si-O-Si angles and Si-O distances is observed in the stable structures of silicates and siloxanes (Libeau, 1985; Tossel and Vaughan, 1992 and references therein). The Density Functional Theory and Electron Localization Function (refer to Appendix B.1 for the methods) were employed to investigate whether the bending of the Si-O-Si angle results in a weakening of the SiO bonds. The electron distribution at the bridging oxygen atom and the stability of the SiO bond with the bending of the Si-O-Si bond angle are studied in the $(OH)_3SiOSi(OH)_3$ molecule (see Appendix C). Most evident electronic effect observed when the Si-O-Si angle is bent is the emergence of a third valence shell-charge concentration region around the bridging oxygen, in addition to the two found along the SiO bonds. Some authors suggest a change in oxygen hybridization from *sp* to sp^2 with bending, despite the absence of a third atom coordinating the central O atom (Downs, 1995). The structural consequences of the change in oxygen hybridization from *sp* to sp^2 are analyzed in the Section 7 for the high-pressure-driven transition from the tridymite SiO_2 polymorph to the stishovite SiO_2 polymorph.

A comprehensive study on the stability of the SiO bond with Si-O-Si angle bending is provided in Appendix C. In summary, this study indicates that: 1) Deviation of the Si-O-Si angle from 180° leads to a

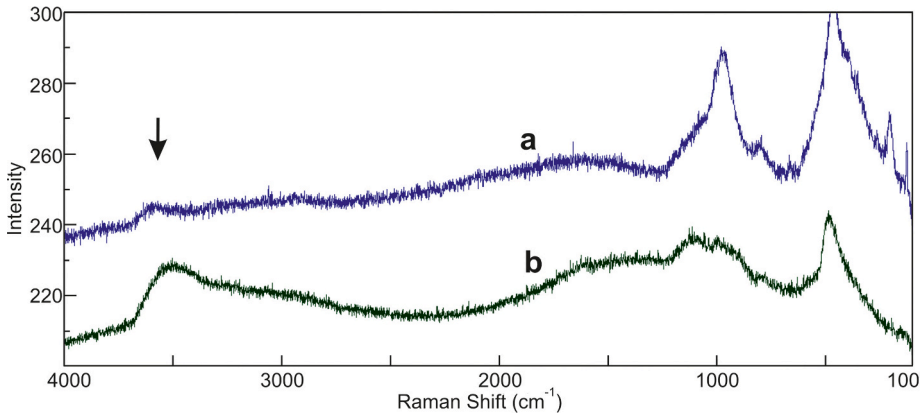

Fig. 4. Raman spectra of the glass formed around the quartz pellets (Fig. 2F) in Experiment B-1 (A), and of the glass occurring within the regions occupied by the precursor quartz pellets (Fig. 2E) in Experiment B-2 (B).

progressive concentration of electron charge at the SiO interatomic region. 2) However, the concentration of electronic charge in the binding region is limited. 3) At the limit, for small Si-O-Si angles, the electron density is removed from the binding region, and accumulates in the antibinding regions. The consequence of these phenomena is that valence electrons are promoted to high-energy SiO antibonding states, leading to a weakening of the SiO bond.

6. Effect of electron count on the structure of quartz

The impact of alkalis on silicate depolymerization, which is significant at low pressure, is not as pronounced at high pressure (Hirschmann et al., 1998). This section addresses the population of SiO antibonding orbitals by adding extra valence electrons (increasing electron count) to the structure of quartz. This approximates the effect of alkali electron donor atoms on the depolymerization of silicates.

Density Functional Theory (DFT) calculations and Quantum Theory of Atoms in Molecules (QTAIM) analysis were performed on the quartz crystal structure, where it was modified by adding two extra valence electrons (Appendix B.2). They reveal a significant increase in interatomic distances, volume and number of valence electrons of Si with the increase of valence electrons (Table 2). In contrast to Si, the volume and number of valence electrons of O increase moderately. The intertetrahedral (Si-O-Si) angle also increase slightly with the addition of valence electrons. Calculations further indicate a drastic distortion of silica tetrahedra with the addition of extra valence electrons (Table 2).

The addition of two extra valence electrons to the structure of quartz resulted in a geometrical effect that extends the Si-O bond distances due to a significant increase in the volume of Si atoms. The extension of Si-O bond distances enhances the compressibility of quartz, as longer bonds are more compressible than the shorter ones. As the structure expands and the Si-O bond distances lengthen, the electron density is removed from binding region. The lowest-energy empty orbitals in the structure of quartz are SiO antibonding and have a substantial Si character (Tossel and Vaughan, 1992). These antibonding orbitals are now populated because they stabilize with the increase in bond distance (the stabilization of antibonding orbitals results from the combination of empty outer atomic orbitals, which overlap at larger distances than inner atomic orbitals). Finally, electronegativity of silicon increases drastically with electron count, which would favor Si-O-Si bending. This is because for constant B, the A-B-A angle decreases as A becomes more electronegative (Tossel and Vaughan, 1992).

The incorporation of K^+, Na^+ and Ca^{2+} into the three-dimensional structure of quartz based in the linkage between six-fold rings is accompanied by the replacement of a silicon cation (Si^{4+}) with an aluminum cation (Al^{3+}). This replacement results in major bond distances with O in the structure of feldspars, which are based on the linkage between four-fold rings. As demonstrated in the rationale, a measure of the population of high-energy SiO antibonding orbitals is the number of valence electron per atom (or electron count; Burdett, 1980, page 265). The electron count varies from 5.82 in albite to 6.4 in anorthite, with a value of 5.33 for quartz. The predominance of six-membered rings over three- or four-membered rings in nature was attributed early by Pauling (1929) to the fact that the 120° angle in the six-membered rings approximates a tetrahedral angle. This assertion applies if the Si-O-Si angle is fixed at 180°. Coesite, one of the high-pressure polymorphs of the SiO_2, and feldspars have quite similar structures based on the linkage between four-fold rings and the occurrence of crankshafts (Fig. 5). Thus, high-polymerized silicate structures with 6-membered rings form structures with 4-membered rings due to the increase of the electron count (feldspars) or pressure (coesite).

Table 2
Interatomic distances (*d*SiO, in Å), Si-O-Si and O-Si-O angles, atomic volumes (Å^3) and number of valence electrons of O (2 core electrons and 6 valence electrons) and Si (10 core electrons and 2 valence electrons) for the normal electronic structure of quartz (electronic configuration referred as 0). The same parameters have also been calculated for an electronic configuration with two additional valence electrons (here referred as −2).

	0	*–2*
dSiO	1.62	1.8
Si-O-Si angle	143.2	162.8
O-Si-O angle	108.8–110.8	103.6–116.2
O volume	17.74	26.65
Si volume	2.98	7.68
O valence electrons	7.61	7.65
Si valence electrons	0.79	1.36

7. Oxygen hybridization and O arrangement in tridymite and stishovite structures

Table 3 illustrates a gradual decrease in atomic charges for Si and bridged O, regardless of the type of charge calculated (Mulliken or Bader charges), coinciding with the bending of the Si-O-Si angle for the $(OH)_3Si\text{-}O\text{-}Si(OH)_3$ molecule. Consequently, a decrease in atomic charges is observed when the hybridization of oxygen deviates from the *sp* end member hybrid. A formal shift in oxygen hybridization from *sp* to sp^2 is noted during high-pressure-driven transition from tridymite to stishovite. Table 4 shows that it consists in a decrease of: 1) SiO bond strength, 2) atomic charges and 3) O 2 *s* atomic population. Lower O and Si atomic charges and SiO bond populations measured for stishovite (Table 4) are interpreted as: 1) a depopulation of the SiO bonding and O nonbonding molecular orbitals, which are close in energy to the low-energy O atomic orbitals, and 2) an electron population of SiO

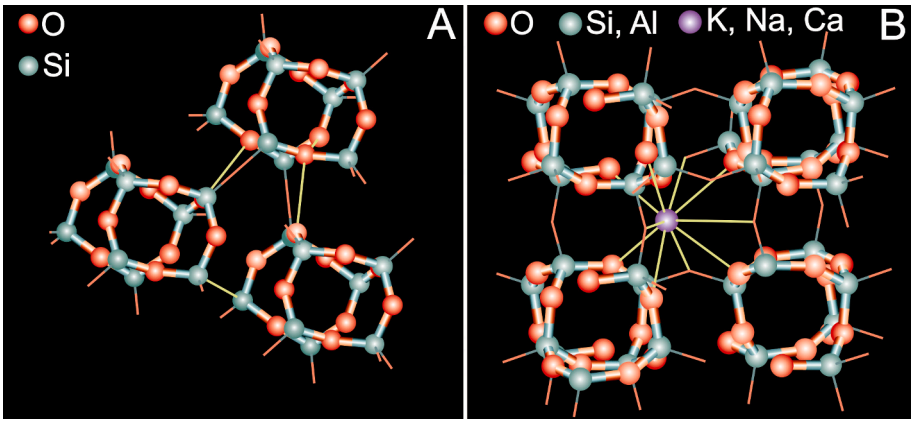

Fig. 5. Sketch of crystal structures of the coesite (A) and feldspar (B) view along the crankshaft-like chains.

Table 3
Mulliken and Bader charges (in *e* units) as a function of Si-O-Si angle calculated for Si and bridged O atoms in $(OH)_3Si\text{-}O\text{-}Si(OH)_3$ molecule (1.60 Å and 1.80 Å values of *d*SiO are used in the calculation of Mulliken and Bader charges, respectively).

	Mulliken charges (dSiO = 1.60 Å)		*Bader charges (dSiO = 1.80 Å)*	
SiOSi angle	*Si*	*O*	*Si*	*O*
180°	1.60	−1.03	3.15	−1.54
160°	1.52	−0.96	3.14	−1.53
140°	1.36	−0.83	3.13	−1.51
120°	1.13	−0.68	3.12	−1.48

Table 4
Range of values found for the O and Si Mulliken charges, SiO bond populations, charge difference at the middle point between two adjacent oxygens, ΔρOO, (deformation density, in *e* units), Si-O and O-O interatomic distances, *d*SiO and *d*OO respectively, (in Å) for the tridymite (Dollase and Baur, 1976) and stishovite (Ross et al., 1990) structures.

	Tridymite	*Stishovite*
O charges	−1.18 to −1.21	−1.01
Si charges	2.35–2.42	2.02
O 2 s atomic population	1.81–1.83	1.80
dSiO	1.554–1.647	1.756–1.813
SiO bond populations	0.51–0.56	0.38–0.46
dOO	2.55–2.68	2.29–2.66
ΔρOO	−0.08 to −0.2	−0.08 to −0.2

antibonding molecular orbitals, which are close in energy to the empty high-energy Si atomic orbitals. It also results in a decrease of the ionization energy of the frontier orbitals, and therefore, in an increase of the "oxygen basicity" in the stishovite SiO_2 polymorph.

Table 4 also demonstrates a reduction in O-O distances when transitioning from the low-pressure tridymite structure to the high-pressure stishovite structure. Consequently, OO interactions have been examined in tridymite and stishovite structures. Comparable values of deformation density in the OO interatomic region (ΔρOO; Appendix B.3) are observed in both the tridymite and stishovite structures (Table 4). This suggests that the nonbonded repulsion between O atoms did not intensify, despite the anticipated increase in OO overlap associated with the rise in the coordination number from 6 to 12 and the shortening of O-O distances from tridymite to stishovite.

According to the principles outlined by Laves, the highest symmetry, highest coordination numbers, and dense packing of atoms should be evident in the geometries of ionic and metallic crystals. While our interest lies in the explaining bond angle geometries as a consequence of covalent effects, we will next consider oxygen atoms as spherical entities, akin to billiards balls. Fig. 6 presents a projection of the oxygen sub-lattices of the ideal tridymite and stishovite structures. In tridymite, the oxygen sublattice forms a partially occupied close-packed arrangement (with either 3/4 or 1/4 of the positions is occupied, depending on the layers) of small and separated spheres (Fig. 6A). Next-nearest-neighbor O atoms cannot interact, except through their nearest neighbors, the Si atoms. The packing of the oxygen atoms follows a regular sequence of the type **…abacabac…** with 3/4 of the positions in layers **a** occupied, and 1/4 in layers **b** and **c**. The displacements, indicated by arrows in Fig. 6A, of the atoms from layers **a** to unoccupied positions in layers **b** and **c,** result in a true of close packing of oxygen atoms. This packing follows a sequence of the type **…bcbc…**, similar to that observed in the stishovite structure (Fig. 6B). In the projection shown in Fig. 6A, two arrows are depicted per sphere in layer **a**, one arrow for each oxygen atom in the two layers **a,** which are necessary to form the close-packing of one layer **b** and of one layer **c** (1/4 of the positions occupied in **b**, or **c**, plus 3/4 of the positions occupied in **a**).

The proposed reconfiguration of the oxygen sublattice, anticipated for the transition from tridymite to stishovite structure, is likely facilitated by the softening of the oxygen atoms, depicted as larger spheres in Fig. 6. The shorter homonuclear (O-O) distances within the stishovite structure can be attributed to an enhancement of the polarization (correlation) forces between the softer O atoms (weak OO interactions). This enhancement results from the shift in oxygen hybridization from *sp* to sp^2, which is accompanied by bending of the Si-O-Si angle and elongation of the of Si-O distances.

8. Discussion

8.1. Robustness of zircon

Zircon can survive processes like weathering and metamorphism (Fedo et al., 2003). The resistance of zircon, in comparison to other nesosilicates, stems from the robust bonds between Zr and O (Velbel, 1999). As demonstrated in the rationale, a covalent stabilization arises from the interaction between an electronegative cation (soft acid) and an electropositive anion (soft base). This covalent stabilization of the SiO_4^{4-}-Zr^{4+} soft-soft pair likely promotes the formation of zircon across a wide *P-T-X* range. A similar phenomenon is observed for almandine garnet, which can form at relatively low pressures because of the strong stabilizing effect of iron. The partitioning of Fe and available Mn into garnet results in a significant expansion of its stability field (Spear, 1995, pages 340 and 353). Moderately electronegative Zr atoms form covalent bonds with less electronegative oxygen atoms in the zircon structure. Conversely, the more Si-O-Si links present in a silicate structure, the greater electronegativity of the oxygen atoms attached to the metallic ions (Ramberg, 1952).

Our experimental findings indicate that the formation of zircon,

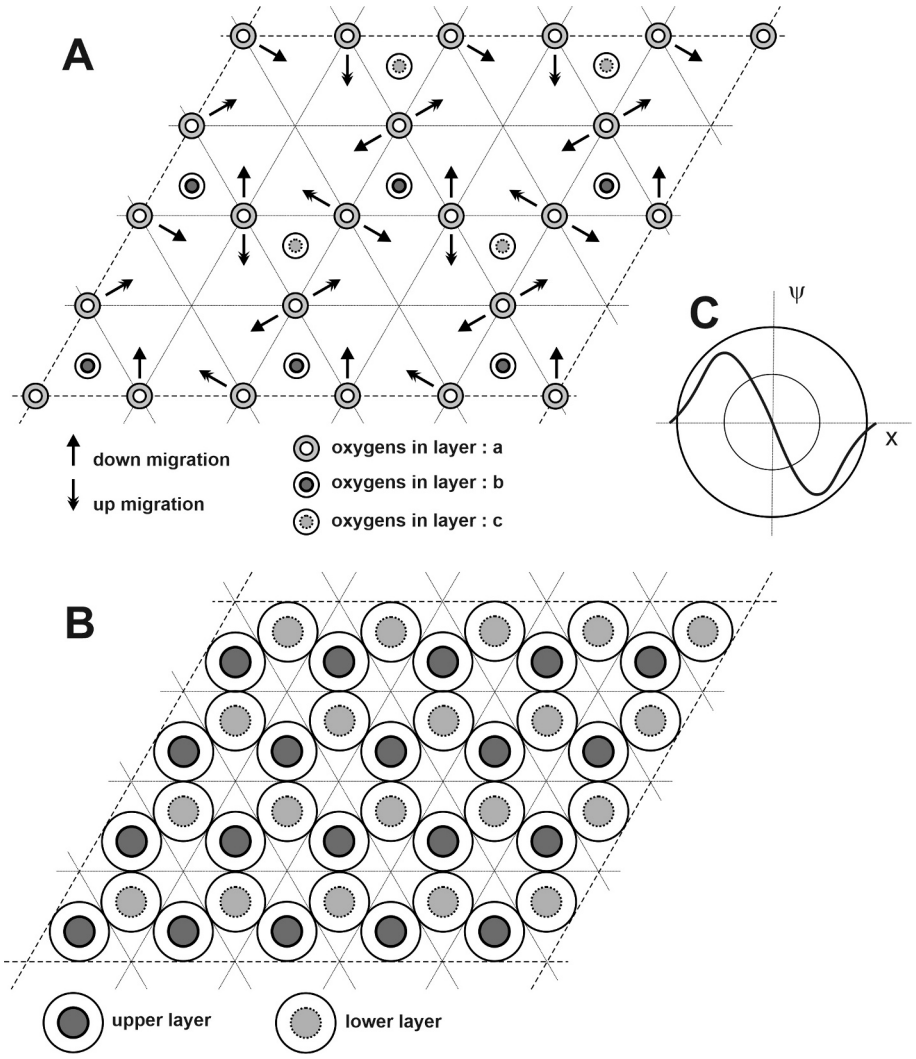

Fig. 6. A) Sketch of the oxygen sublattice of an ideal tridymite forming a pseudo-close-packed arrangement with the **… c a b a c …** stacking sequence for oxygen atoms (only 3/4 and 1/4 of positions are occupied, depending on the layers). Migration of O atoms from layers **a** to layers **c** and to layers **b** are represented by arrows. B) Sketch of the oxygen sublattice forming a close-packed arrangement with the stacking sequence **… c b c b c…** obtained after the rearrangement of O atoms shown in (A). Close-packed arrangement of the oxygen anions within the stishovite structure is allowed by an improvement of the polarization (correlation) forces between softer O atoms here represented by larger spheres. C) O *p* valence electrons are represented by a stationary wave having a wavelength equal to the diameter of the sphere.

characterized by a distorted close packed structure of oxygen atoms, and the melting of quartz, which has an open framework structure, are both facilitated by pressure. Additionally, water plays an essential role in these processes. The application of pressure brings atoms closer together, resulting in an increase in coordination number and a decrease in Si-O-Si links in silicates with structures that have tightly bonded SiO_4^{4-} groups.

There is also a transition in oxygen-sublattice packing from tectosilicates (*e.g.* quartz) to nesosilicates (*e.g.* olivine). Both pressure, through Si-O-Si bond angle bending, and the addition of extra valence electrons lead to lengthening of Si-O bond distances. The weakening of SiO bonds reduces the degree of polymerization through -O- bridges in the Si-O frameworks, favoring a close-packed array of oxygen atoms where the available tetrahedral voids are occupied by the Si atoms.

The structure of olivine, and to a lesser extent that of zircon, may be viewed as an assembly of oxygen atoms arranged in a close-packet configuration (hexagonal and cubic, respectively), held together by cations. In the structure of olivine, silicon and magnesium are located in the tetrahedral and octahedral interstices, respectively, of the close-packed oxygen assembly.

The radius of Zr^{4+} is no larger than that of Mg^{2+}, but its higher polarizing power induces a significant distortion of the oxygen arrangement. The substitution of Mg^{2+} by Zr^{4+}, which has a high polarizing power and forms covalent bonds with oxygen atoms, affects physical properties of the nesosilicate. This results in a less tightly packed arrangement of oxygen atoms in the zircon structure compared to the olivine structure.

The structural control of the physical properties of silicates is particularly influenced by the type of grouping of the silica tetrahedra. However, the substitution of Si^{4+} by electronegative cations as non-Si^{4+} tetrahedral occupants would maintain the structural backbone, which would have virtually no impact on mineral's physical properties (Bloss, 1994, page 273). The substitution of Si^{4+} by Zr^{4+} in Si_2O_4 preserves covalent bonding and prevents the occurrence of true close-packing of oxygen atoms in the silicate structure. Therefore, zircon serves as an example of a robust covalent structure that is stabilized under high pressure.

8.2. Discontinuous Bowen's reaction series

The depolymerization process in silicates follows the discontinuous Bowen's reaction series: SiO_2^0 (framework silicates) → $Si_4O_{10}^{4-}$ (layer silicates) → $Si_4O_{11}^{6-}$ (double-chain silicates) → SiO_3^{2-} (single-chain and ring silicates) → $Si_2O_7^{6-}$ (double-island silicates) → SiO_4^{4-} (island silicates). The percentage of bridging oxygens varies from zero for isolated tetrahedra, 14.3 for double tetrahedra, 33.3 for single chains and for rings, 45.5 for double chains, 60 for sheets, and 100 for frameworks (Bloss, 1994, page 266). If pressure results in the breaking of the SiO bonds through the bending of the Si-O-Si bond angle, as inferred from our discussion, the decrease in the Si:O ratio from tectosilicates to nesosilicates must be associated with the increase in pressure affecting Earth's materials with depth.

The discontinuous Bowen's reaction series is associated with an increase in the basicity of oxygen atoms, which we believe favors their packing. As previously indicated, the bending of the Si-O-Si angle, along with the increase in Si-O interatomic distances, promotes new covalent or overlap stabilizing interactions. This leads to a higher occupation of ligand orbitals surrounding central O atoms and to a lower occupation of O atomic orbitals, thereby resulting in lower O and Si atomic charges. Although O and Si atoms become more alike with Si-O-Si bending (Table 3) the oxygen atom remains more electronegative than the Si atom, and its potential well is always stronger. The stability of the SiO bonds can be verified by the electron-binding energy in the bridging oxygen atoms. This electron binding energy corresponds to the ionization potential of the electrons found in HOMO orbitals. The increase in the energy of the siloxane molecule associated with the Si-O-Si bending and the partial decrease of energy with Si-O distance (Appendix Fig. 2B) reflects the evolution of the frontier molecular orbitals, the antibonding $2\sigma_g$ orbital and the O p $1\pi_u$ orbital, with the change of the Si-O-Si angle and Si-O distance (Tossel and Vaughan, 1992). The stabilization of one part of the O p $1\pi_u$ orbital with Si-O-Si bending ($2a_1$ in the bent geometry) may be related to an improvement in covalent stabilization. Furthermore, the increase of the Si-O distance stabilizes the antibonding $3a_1$ orbital, which favors the population of SiO antibonding orbitals (Tossel and Vaughan, 1992). This final effect manages the decrease in the ionization energy of the frontier orbitals with the Si-O-Si angle bending and the increase of the Si-O distance, and therefore, results in an increase in the basicity and the electropositive character of the bridged oxygen.

8.3. Continuous Bowen's reaction series

In addition to pressure, the composition of the system can alter the nature of the oxygen in the silicate structure (electronegativity perturbation). For example, substituting Si with Al results in anion softening in the silicate crystals and melts. The continuous Bowen's reaction series can also be interpreted as a progressive change in the basicity of the oxygen atoms in the aluminosilicates. The substitution of Si^{4+} by Al^{3+} leads to variations in bond lengths and physicochemical properties. Consequently, the decomposition of plagioclase by acids increases with the aluminum content (Gutmann, 1978, page 62), which is explained by the increased basicity of their oxygen atoms. An increase in refractive index results from the closer packing of atoms (oxygen atoms in the case of silicates) and/or from greater polarizability (Bloss, 1994, page 439). The increase in the refractive index in plagioclase with substitution of Si^{4+} by Al^{3+} correlates with the increase in the electron count and basicity of the oxygen atoms (electron count varies from 5.82 in albite to 6.4 in anorthite).

8.4. "Metallization" in rocky planets

The effect of pressure on the materials that form planets, which naturally increase their density, can be described by the so-called "pressure-distance paradox" (Gutmann, 1978, page 66). According to this paradox, an increase in pressure results in an elongation of the shortest intra-molecular distances in soft (weakly bound) materials that form giant gas planets and a significant reduction of their large inter-molecular distances. A similar phenomenon also occurs in stiff (tightly bound) materials that form rocky planets. For these materials, an increase in the coordination number of chemical elements in their ionic and covalent structures with pressure leads to an elongation of the bonds between nearest-neighbor atoms. The decrease in the ratio of next-nearest-neighbors to nearest-neighbors distances leads to a structural compaction process known as "metallization" (Burdett, 1995, page 148). Inorganic materials with ionic or covalent structures or organic materials with molecular lattice structures are transformed into a metallic state by application of sufficiently high pressure. The occurrence of metallic character in the periodic table of elements depends on the ambient conditions imposed on the planets (Edwards and Sienko, 1983). In more compressible molecular lattices, the distinction between inter-molecular and intra-molecular bonds is easily made. In less compressible coordination structures, like those of silicate minerals and melts, an increase in pressure leads to an increase of bond distances (*e.g.* Si-O distances) when the coordination number increases. However, the resulting shorter homonuclear (*e.g.* O-O distances) distances within the structure are usually not considered as chemical bonds. Pressure significantly shortens the distance between next-nearest-neighbors, leading to a geometrical rearrangement with an increase in coordination number (Kushiro and Mysen, 1992; Kelsey et al., 2009).

The structure defined by the oxygen sublattice of the silicates evolves from open structures at the Earth's surface to more densely packed structures toward the Earth's interior. In a study on the silicate structure, Bragg (1930) argued that only nearest-neighbor forces bind atoms together in a coordinated polyhedron, and that next-nearest-neighbor atoms can interact only through their nearest neighbors. However, Pantelides (1975) demonstrated that for closely packed arrangements, such as those observed in rock-salt-type compounds, the dominant atomic interactions occur between anions. This contrasts with open structures such as zinc-blende-type materials where only nearest anion-cation interactions are considered. The electronic structure of the close-packed anion sublattice resembles the electronic structure of the inert-gas solids, which essentially mirrors the electronic structure of isolated atoms (Pantelides, 1975; Harrison, 1989, page 297). Non-polar molecules, anions, rare-gas and oxygen atoms weakly attract each other through the so-called Van der Waals interaction, which is a manifestation of correlation energy. Van der Waals forces increase from the Ne solids to other inert-gas solids formed by noble-gas elements of higher atomic size and lower ionization energy, such as Ar or Kr.

Pantelides (1975) also elucidated the relationship between the ionization energy of rare-gas elements and their interatomic distances in solids. This was achieved by considering the atom as a sphere and the valence p state as a wave with wavelength equal to the diameter (d) of the sphere: The potential energy of the state results in an ionization energy or electron binding energy equal to $\eta_g \hbar^2 / \left(md^2\right)$, where h is Planck's constant, η_g is a constant depending of the type of atoms (inert-gas elements or ions) and m the mass of the electron. As indicated in Section 8.2, the stabilization of the antibonding $2\sigma_g$ orbital with the increase of the Si-O distance promotes Si-O-Si bending. This is equivalent to a hypothetical destabilization of the O p $1\pi_u$ orbital. Electronic interactions between bridging oxygens of Si-O-Si network structures are comparable to those occurring between rare-gas elements. Following the earlier discussion, a wave may be assigned to the O p valence state with a wavelength equal to the interatomic distance between Si and O atoms. Interestingly, the ionization or electron-binding energy of an atom is related here to an interatomic distance. The decrease in the ionization potential of the bridging oxygens due to the hypothetical destabilization of the O p $1\pi_u$ orbital with Si-O distance must increase their atomic volumes and enhance polarization or correlation forces between the oxygens. These forces would also be responsible for the decrease of the

O-O distances between the oxygen atoms in stishovite compared to tridymite (Table 4).

The sizes of the spheres in Fig. 6A-B qualitatively correspond to the "hypothetical" diameters of O atoms in tridymite and stishovite, respectively. The energy required to remove an electron from an O ion (electron affinity) is related to *d*SiO in the solid. As demonstrated for inert-gas solids, this result can be rationalized by conceptualizing the O atom as a sphere and the O *p* valence electrons as a stationary wave (Fig. 6C). This wave has a wavelength equal to the Si-O interatomic distance in the solid.

8.5. Pressure dependence of dry and hydrous melting

In addition to the structural changes previously discussed, significant physicochemical consequences arise from the change in the polarizability of oxygen anions due to alterations in their coordination environment. A decrease in oxygen hybridization results in anion softening, which prompts next-nearest-neighbor atoms to interact directly. In this section, the pressure-temperature dependence of silicate melting curves under both wet and dry conditions is explained by nearest-neighbor and next-nearest-neighbor forces in the structure, respectively.

Our theoretical approach reveals a significant increase in the energy of the SiO bonds as the Si-O-Si angle bends. Experimental evidence suggests that the melting of quartz in the presence of water occurs at high pressure. Accordingly, the *P-T* relationship observed for the wet solidus is governed by the stronger nearest-neighbor interactions within the Si-O-Si "skeleton" that forms the high-polymerized silicate crystals (*e.g.* quartz). In this scenario, the melting temperature decreases with increasing pressure (as shown in the left-hand curve of Fig. 7A). This is because of the bending of the Si-O-Si bond angle with increasing pressure facilitates an acidic attack by the hydrogen of water onto the softer (more basic) bridging O atoms of weaker of SiO bonds.

Conversely, the pressure-temperature *P-T* dependence of dry solidus is governed by the enhancement of OO polarizing interactions, which are favored by the weakening or breaking of the SiO bonds in the silicate structures as pressure increases. Consequently, the melting temperature rises with pressure (as depicted in the right-hand curve of Fig. 7A). The stabilization of the solid with increasing pressure is associated with the strengthening of weak next-nearest-neighbor forces. To comprehend this, the arrangement of oxygen atoms in the anion sub-lattices of silicates is once again compared to the structure of inert-gas solids. The *P-T* melting curves obtained by Jephcoat and Besedin (1998) for rare gas solids (Fig. 7B) demonstrate how noble gas atoms are more strongly bound together with increasing atomic size and pressure. The binding energy between atoms escalates with increasing atomic size, stabilizing noble gas atoms within the solid lattice. The decrease in the ionization energy noble gas atoms enhances the binding energy in inert-gas solids. Similarly, the decrease in the electron affinity of oxygen atoms amplifies OO polarizing interactions in the anion sub-lattices of silicates as pressure increases. The softening of the oxygen atoms, which improves OO polarizing interactions, is more pronounced in more basic or depolymerized systems of silicate composition. This explains the stabilization of the solid state and the shift of the peridotite melting curve to higher temperature compared to the granite curve.

9. Conclusions

Quantum mechanical calculations and laboratory experiments have been performed to elucidate the depolymerization processes in silicates. Tridymite and quartz were selected as representative examples of highly polymerized structures with Si-O-Si links and short bonds between tetrahedrally-coordinated Si and oxygen atoms. These two minerals exhibit covalent structures that are stable under low pressure. In contrast, stishovite and zircon were chosen as examples of depolymerized silicates. The structure of zircon does not contain any Si-O-Si links, whereas the structure of stishovite does contains Si-O-Si links but with extended Si-O bond distances. Both minerals also possess covalent structures, but they are stable under high pressure.

Theoretical calculations enabled us to analyse the destabilization of the SiO bond associated with Si-O-Si bond-angle bending, which is related to pressure. We have also investigated the elongation of Si-O bond distances in relation to the increase in the electron count of the system, which approximates the impact of alkali electron donor atoms on the depolymerization of silicates. Our findings suggest that depolymerization primarily occurs as result of increased pressure and is accompanied by a change in oxygen hybridization, a reduction in O-O distances, improved OO bonding interactions and enhanced packing of the oxygen sublattice in the silicate structures. All these effects result in an increase in the "size" (and basicity-polarizability) of the oxygens.

Moreover, the depolymerization reaction 1 quartz +1 baddeleyite → 1 zircon can be viewed as a proxy for the acid-base reaction $O^0 + O^{2-} \rightarrow 2O^-$. This suggests that the precipitation of zircon and the melting of quartz under pressure lead to an increase in the basicity of oxygen atoms. The bending of the Si-O-Si angle due to increased pressure intensifies the acid attack by water's hydrogen ions on the bridging oxygen anions in the quartz structure. The driving force for zircon crystallization originates from the covalent interaction between Zr^{4+} (an electronegative cation or soft acid) and a less electronegative oxygen anion (or

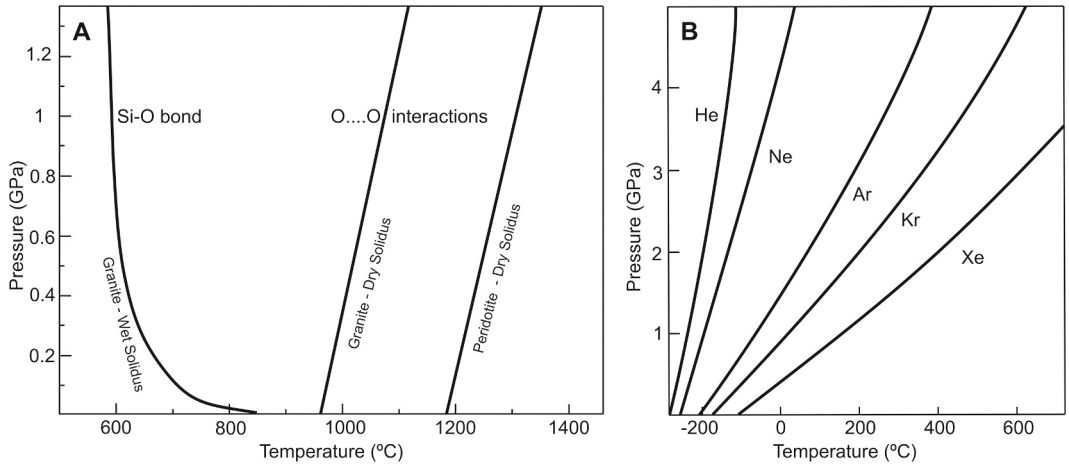

Fig. 7. A) Change of solidus temperature with pressure for silicates. It is indicated the granite dry and hydrous melting curves (Johannes and Holtz, 1996) as controlled by weak O-O interactions and strong Si-O-Si bonds, respectively. Peridotite melting curve is also represented. B) *P-T* melting curves for rare gas solids (from Jephcoat and Besedin, 1998).

softer base) that results from the high pressure melting of quartz. However, zircon is not a typical nesosilicate. The true close-packed oxygen arrangement observed in most (ionic) structures of the nesosilicate group is not present in zircon. Silicate minerals with covalent structures, such as zircon or quartz, are resistant to weathering, chemical, and mechanical abrasion under Earth's surface conditions. Furthermore, zircon can also withstand metamorphism. Pressure, which facilitates the dissolution of quartz due to its open structure, does not affect zircon.

CRediT authorship contribution statement

A. Sánchez-Navas: Investigation. **S. Melchor:** Investigation. **J. Ortega-Castro:** Investigation. **I. Vidal-Daza:** Investigation. **A. Castro:** Investigation.

Declaration of competing interest

Antonio Sanchez-Navas reports was provided by University of Granada. If there are other authors, they declare that they have no known competing financial interests or personal relationships that could have appeared to influence the work reported in this paper.

Data availability

No data was used for the research described in the article.

Acknowledgements

This work is a contribution of the research group RNM-179 of the Junta de Andalucía, Spain. ASN and AC wish to express their gratitude for the financial support received from projects CGL2012-32169 and PID2021-126347NB-I00.

Appendix A. Supplementary data

Supplementary data to this article can be found online at https://doi.org/10.1016/j.chemgeo.2024.122156.

References

Bader, R.F.W., 1990. Atoms in Molecules. Clarendon Press, Oxford, p. 456.
Bea, F., Bortnikov, N., Cambeses, A., Chakraborty, S., Molina, J.F., Montero, P., Morales, I., Silantiev, S., Zinger, T., 2022. Zircon crystallization in low-Zr mafic magmas: possible or impossible? Chem. Geol. 602, 120898.
Bloss, F.D., 1994. Crystallography and Crystal Chemistry. An Introduction. Mineralogical Society of America, Washington, p. 545.
Bragg, W.L., 1930. The structure of silicates. Nature 125, 510–511.
Brown, G.E., Gibbs, G.V., 1969. Oxygen coordination and the Si-O bond. Am. Mineral. 54, 1528–1539.
Burdett, J.K., 1980. Molecular shapes: Theoretical Models of Inorganic Stereochemistry. John Wiley & Sons, New York, p. 287.
Burdett, J.K., 1995. Chemical Bonding in Solids. Oxford University Press, New York, p. 319.
Burdett, J.K., McLarnan, T.J., 1984. An orbital interpretation of Pauling's rules. Am. Mineral. 69, 601–621.
Burnham, C.W., 1975. Water and magmas: a mixing model. Geochim. Cosmochim. Acta 39, 1077–1084.
Connolly, J.A.D., 2023. A Collection of Fortran77 Programs for Calculating Phase Diagrams, Manipulating Thermodynamic Data, and Modeling Equilibrium Phase Fractionation and Reactive Transport. https://www.perplex.ethz.ch.
DeKock, R.L., Barbachyn, M.R., 1979. Proton affinity, ionization energy, and the nature of frontier orbital electron density. J. Am. Chem. Soc. 101, 6516–6519.
Dekock, R.L., Gray, H.B., 1989. Chemical Structure and Bonding. University Science Books, Sausalito, p. 491.
Dera, P., Lazarz, J.D., Prakapenka, V.B., Barkley, M., Downs, R.T., 2011. New insights into the high-pressure polymorphism of SiO_2 cristobalite. Phys. Chem. Miner. 38, 517–529.
Dollase, W.A., Baur, W.H., 1976. The superstructure of meteoritic low tridymite solved by computer simulation. Am. Mineral. 61, 971–978.
Downs, J.W., 1995. Electron density and electrostatic potential of coesite. J. Phys. Chem. 99, 6849–6856.
Edwards, P.P., Sienko, M.J., 1983. On the occurrence of metallic character in the periodic table of the elements. J. Chem. Educ. 60, 691–696.
Fedo, C.M., Sircombe, K.N., Rainbird, R.H., 2003. Detrital zircon analysis of the sedimentary record. Rev. Mineral. Geochem. 53, 277–303.
Fyfe, W.S., 1954. The problem of bond type. Am. Mineral. 39, 991–1004.
Gutmann, V., 1978. The Donor-Acceptor Approach to Molecular Interactions. Plenum Press, New York, p. 279.
Harrison, W.A., 1989. Electronic Structure and the Properties of Solids. The Physics of the Chemical Bond. Dover Publications, New York, p. 585.
Hazen, R.M., Finger, L.W., Hemley, R.J., Mao, H.K., 1989. High-pressure crystal chemistry and amorphization of α-quartz. Solid State Commun. 72, 507–511.
Hess, P.C., 1977. Structure of silicate melts. Can. Mineral. 15, 162–178.
Hirschmann, M.M., Baker, M.B., Stolper, E.M., 1998. The effect of alkalis on the silica content of mantle-derived magmas. Geochim. Cosmochim. Acta 62, 883–902.
Jensen, W.B., 1980. The Lewis Acid-Base Concepts: An Overview. Wiley, New York, p. 364.
Jensen, W.B., 1996. Electronegativity from avogadro to pauling: part 1: origins of the electronegativity concept. J. Chem. Educ. 73, 11–20.
Jephcoat, A.P., Besedin, S.P., 1998. Melting of rare gas solids Ar, Kr, Xe at high pressures and fixed points in the P-T plane. In: Manghnani, M.H., Yagi, T. (Eds.), Properties of Earth and Planetary Materials at High Pressure and Temperature, Geophysical Monograph Series 101, Washington D.C, pp. 287–297.
Johannes, W., Holtz, F., 1996. Petrogenesis and Experimental Petrology of Granitic Rocks. Minerals and Rocks Series Vol. 22. Springer-Verlag, Berlin, p. 335.
Kelsey, K.E., Stebbins, J.F., Mosenfelder, J.L., Asimow, P.D., 2009. Simultaneous aluminum, silicon, and sodium coordination changes in 6 GPa sodium aluminosilicate glasses. Am. Mineral. 94, 1205–1215.
Koch-Muller, M., Fei, Y., Hauri, E., Liu, Z., 2001. Location and quantitative analysis of OH in coesite. Phys. Chem. Miner. 28, 693–705.
Kushiro, I., 1975. On the nature of silicate melt and its significance in magma genesis: regularities in the shift of the liquidus boundaries involving olivine, pyroxene, and silica minerals. Am. J. Sci. 275, 411–431.
Kushiro, I., Mysen, B.O., 1992. A possible effect of melt structure on the Mg–Fe^{2+} partitioning between olivine and melt. Geochim. Cosmochim. Acta 66, 2267–2272.
Le Losq, Ch., Neuville, D.R., Moretti, R., Roux, J., 2012. Water quantification and speciation in silicate melt using Raman spectroscopy. Am. Mineral. 97, 779–791.
Lenoir, M., Grandjean, A., Linard, Y., Cochain, B., Penelon, B., Neuville, D.R., 2008. The influence of the Si, B substitution and of the nature of network modifying cations on the properties and structure of borosilicate glasses and melts. Chem. Geol. 256, 316–325.
Libeau, F., 1985. Structural Chemistry of Silicates: Structure, Bonding, and Classification. Springer-Verlag, New York, p. 368.
Mulliken, R.S., Pearson, W.B., 1969. Molecular Complexes. A Lecture and Reprint Volume. Wiley Interscience, New York, p. 498.
Neuville, D.R., Cormier, L., Montouillout, V., Florian, P., Millot, F., Rifflet, J.C., Massiot, D., 2008. Structure of Mg- and Mg/Ca aluminosilicate glasses: ^{27}Al NMR and Raman spectroscopy investigations. Am. Mineral. 83, 1721–1731.
Pantelides, S.T., 1975. Universal valence bands for rocksalt-type compounds and their connection with those of tetrahedral crystals. Phys. Rev. B 11, 5082–5093.
Pauling, L., 1929. The principles determining the structure of complex ionic crystals. J. Am. Chem. Soc. 51, 1010–1026.
Pearson, R.G., 1966. Acids and bases. Science 151, 172–177.
Ramberg, H., 1952. Chemical bonds and the distribution of cations in silicates. J. Geol. 60, 331–335.
Ross, N.L., Shu, J.F., Hazen, R.M., Gasparik, T., 1990. High-pressure crystal chemistry of stishovite. Am. Mineral. 75, 739–747.
Ryerson, F.J., 1985. Oxide solution mechanism in silicate melts: systematic variations in the activity coefficient of SiO2. Geochim. Cosmochim. Acta 49, 637–651.
Silvi, B., Wagner, F.R., 1997. The nature of silicon-oxygen bonds in silica polymorphs. In: Silvi, B., D'Arco, P. (Eds.), Modelling of Minerals and Silicated Materials. Kluwer, New York, pp. 179–199.
Spear, F.S., 1995. Metamorphic Phase Equilibria and Pressure-Temperature-Time Paths. Mineralogical Society of America, Washington, p. 799.
Thompson, R.M., Downs, R.T., Dera, P., 2011. The compression pathway of quartz. Am. Mineral. 96, 1495–1502.
Tossel, J.A., Vaughan, D.J., 1992. Theoretical Geochemistry: Applications of Quantum Mechanics in the Earth and Mineral Sciences. Oxford University Press, Oxford, p. 514.
Velbel, M.A., 1999. Bond strength and the relative weathering rates of simple orthosilicates. Am. J. Sci. 299, 679–696.
Walther, J.V., Helgeson, H.C., 1977. Calculation of the thermodynamic properties of aqueous silica and the solubility of quartz and its polymorphs at high pressures and temperatures. Am. J. Sci. 277, 1315–1351.
Wang, Y., Sakamaki, T., Skinner, L.B., Jing, Z., Yu, T., Kono, Y., Park, C., Shen, G., Rivers, M.L., Sutton, S.R., 2014. Atomistic insight into viscosity and density of silicate melts under pressure. Nat. Commun. 5, 3241.